IOP Publishing Journal of Geophysics and Engineering
J. Geophys. Eng. 14 (2017) 1032–1041 (10pp) https://doi.org/10.1088/1742-2140/aa6fe3

Predominant modes for Rayleigh wave propagation using the dynamic stiffness matrix approach

Tarun Naskar and Jyant Kumar[1]

Indian Institute of Science, Bangalore 560012, India

E-mail: tarun.naskar.be@gmail.com and jkumar@civil.iisc.ernet.in

Received 22 November 2016, revised 15 April 2017
Accepted for publication 27 April 2017
Published 30 June 2017

Abstract

In case of *irregular* dispersive media, a proper analysis of higher modes existing in a dispersion plot becomes essential for predicting the shear wave velocity profile of ground on the basis of surface wave tests. In such cases, an establishment of the predominant mode becomes quite important. In the current investigation for Rayleigh wave propagation, the predominant modes have been evaluated by maximizing the normalized vertical displacements along the free surface. Eigenvectors computed from the dynamic stiffness matrix (DSM) approach are analyzed to find the predominant mode. The results obtained are then compared with those reported in the literature. By varying the displacement amplitude ratios of the predominant mode to the other modes, dispersion plots have also been generated from the multichannel analysis of surface waves (MASW) method. The establishment of the predominant mode becomes especially significant, where usually only two to six sensors are employed and the governing (predominant) modal dispersion curve is usually observed rather than several multiple modes, which can be otherwise identified by using around 24 to 48 sensors.

Keywords: dispersion, inverse analysis, nondestructive testing, predominant mode, Rayleigh wave propagation

(Some figures may appear in colour only in the online journal)

1. Introduction

Two surface wave testing techniques, namely, (i) spectral analysis of surface waves (SASW) and (ii) multichannel analysis of surface waves (MASW), are often employed for predicting the shear wave velocity profile of different layers of ground and pavements (Nazarian 1984, Gucunski and Woods 1992, Nazarian and Desai 1993, Ganji *et al* 1998, Park *et al* 1999, Kumar and Naskar 2015). In the SASW method, tests are normally conducted by employing two to six sensors, and dispersion plots are generated for several combinations of source distance and receiver spacing. To obtain the dispersion plots from the SASW tests, the fast Fourier transform of the signals recorded in a time domain is conducted, and the required phase velocity for different frequencies is then evaluated by finding the phase difference between any two chosen signals (Nazarian 1984, Gucunski and Woods 1992, Nazarian and Desai 1993, Kumar and Naskar 2015). The principal phase difference angle between any two adjacent sensors varies between $-\pi$ and $+\pi$. Accordingly, it is often required to add $2\pi N$ for determining the absolute phase difference between the two signals. Kumar and Naskar (2017) proposed a sliding transform so that the problem associated with the phase unwrapping can be resolved. In the MASW method, a large number of closely spaced sensors, typically 24 to 48, are employed (Park *et al* 1999, Xia *et al* 1999). The dispersion plots are subsequently obtained by using different approaches, namely, (i) a two-dimensional Fourier transform of the signals in time and space domains (Nolet and Panza 1976, Gabriels *et al* 1987), (ii) harmonic wavelet transforms of the obtained signals (McMechan and Yedlin 1981, Park *et al* 1998), and (iii) the convolution of the recorded signals by using a stretch function for transforming the observed data to a swept frequency

[1] Author to whom any correspondence should be addressed.

record (Park *et al* 1999). In the SASW method, if not too many combinations of receiver spacing and source distances are adopted, the predominant mode is often observed in the dispersion plot (Nazarian 1984, Gucunski and Woods 1992, Nazarian and Desai 1993). If a soil profile is *regular* dispersive, that is, when the shear wave velocity increases continuously with depth, the fundamental mode becomes generally the predominant mode (Thomson 1950, Haskell 1953, Dunkin 1965). The inversion task for such a case usually remains straightforward. On the other hand, for an *irregular dispersive* soil profile, that is, when a stiff layer lies above relatively soft stratum, then for predicting the correct soil profile, it becomes usually essential to analyze different multiple modes present in the dispersion plots (Jones 1962, Dunkin 1965, Tokimatsu *et al* 1992, Nazarian and Desai 1993, Ganji *et al* 1998, Park *et al* 1999, Xia *et al* 1999, Zomorodian and Hunaidi 2006, Kumar 2011, Kumar and Naskar 2017). When on account of either a lesser number of sensors or limited combinations of receivers' spacing and source distance, it becomes difficult to establish the multiple modal dispersion curves; one alternative is to establish the predominant modal dispersion curve by conducting the forward analysis. The dispersion plot from the analysis is then compared with that determined experimentally in order to predict the shear wave velocity of different layers. In the existing literature, the information is available to compute superposed modes where the vertical displacements of the first m modes are combined to establish the corresponding dispersion curve associated with the mth superposed mode (Tokimatsu *et al* 1992). Furthermore, by using the maximum flexibility coefficient, Zomorodian and Hunaidi (2006) have provided a method to directly compute the predominant mode rather than obtaining the multiple modes on the basis of the root search method. This method, however, considers a vertical load on the free surface rather than the null force vector, which is needed in a root search method. Following the approach of Hossain and Drnevich (1989), Kumar (2011) determined the predominant modes for Rayleigh wave propagation by using the finite difference formulation of the governing partial differential equation. The predominant modes were computed by maximizing the normalized vertical displacement along the free surface. In the present article, by using the dynamic stiffness matrix (DSM), and on the basis of the quadratic eigenvalue formulation of the problem, we first compute multiple modes and then establish the predominant modes. The results obtained from the analysis are then compared with those available from the literature. In addition, by varying the ratio of the energies of the predominant mode to the other modes, dispersion plots are also analyzed using the MASW method. The present study will be especially beneficial where it is difficult to find different multiple modes on account of either a less number of sensors or limited combinations of source distance and receiver spacing; furthermore, the predominant mode usually dictates the dispersion curve.

2. DSM approach

For a particular frequency and wavenumber, consider a planar Rayleigh surface wave (P-SV) propagating in the direction of the positive x-axis. There will be (i) two components of unknown displacements, namely, horizontal displacement (u) in the direction of the propagating wave and vertical displacement (v), and (ii) two components of unknown stresses, namely, shear stress (τ_{zx}) and vertical normal stress (σ_z). These displacements and stress components at the layer interfaces become solely a function of z. On the other hand, the variations of these functions with respect to x and t are considered harmonic, that is, $u = \bar{u}e^{j(\omega t-\kappa x)}$, $v = \bar{v}e^{j(\omega t-\kappa x)}$, $\tau_{zx} = \bar{\tau}_{zx}e^{j(\omega t-\kappa x)}$, and $\sigma_{zx} = \bar{\sigma}_{zx}e^{j(\omega t-\kappa x)}$, where $j = \sqrt{-1}$. Note that the wave is propagating in the positive x direction, and ω and κ refer to the circular frequency and wavenumber, respectively. The terms $\bar{u}$, $\bar{v}$, τ_{zx}, and σ_{zx} become functions of z (depth). In the DSM approach, for a given layer, the relationship between the applied force vector (**F**) and layer displacement vector (**U**) is expressed as follows (Kausel and Roësset 1981):

$$\mathbf{F}_{4x1} = \mathbf{K}_{4x4}\mathbf{U}_{4x1}, \tag{1}$$

where $\mathbf{F}_{4x1} = [\bar{P}_x^u \; i\bar{P}_z^u \; \bar{P}_x^l \; i\bar{P}_z^l]^T$ and $\mathbf{U}_{4x1} = [\bar{u}^u \; i\bar{v}^u \; \bar{u}^l \; i\bar{v}^l]^T$.

The superscripts u and l are associated with the upper and lower interfaces of the layer, and the subscripts x and z indicate the directions in which the external forces act. Following Kausel and Roësset (1981), for a given layer, the local stiffness matrix ($\mathbf{K}^l$) is defined by the equations below.

$$\mathbf{K}^l = 2kG\begin{bmatrix}\mathbf{K}_{11} & \mathbf{K}_{12}\\ \mathbf{K}_{21} & \mathbf{K}_{22}\end{bmatrix} \tag{2}$$

$$\mathbf{K}_{11} = \frac{(1-s^2)}{2D} \times \begin{bmatrix} \frac{1}{s}(C^rS^s - rsC^sS^r) & -(1 - C^rC^s + rsS^rS^s) \\ -(1 - C^rC^s + rsS^rS^s) & \frac{1}{r}(C^sS^r - rsC^rS^s) \end{bmatrix} - \frac{(1+s^2)}{2}\begin{bmatrix}0 & 1\\ 1 & 0\end{bmatrix} \tag{3a}$$

$$\boldsymbol{K}_{22} = \frac{(1-s^2)}{2D} \times \begin{bmatrix} \frac{1}{s}(C^rS^s - rsC^sS^r) & (1 - C^rC^s + rsS^rS^s) \\ (1 - C^rC^s + rsS^rS^s) & \frac{1}{r}(C^sS^r - rsC^rS^s) \end{bmatrix} - \frac{(1+s^2)}{2}\begin{bmatrix}0 & -1\\ -1 & 0\end{bmatrix} \tag{3b}$$

$$\boldsymbol{K}_{12} = \frac{(1-s^2)}{2D}\begin{bmatrix} \frac{1}{s}(rsS^r - S^s) & -(C^r - C^s) \\ (C^r - C^s) & \frac{1}{r}(rsS^s - S^r) \end{bmatrix} \tag{3c}$$

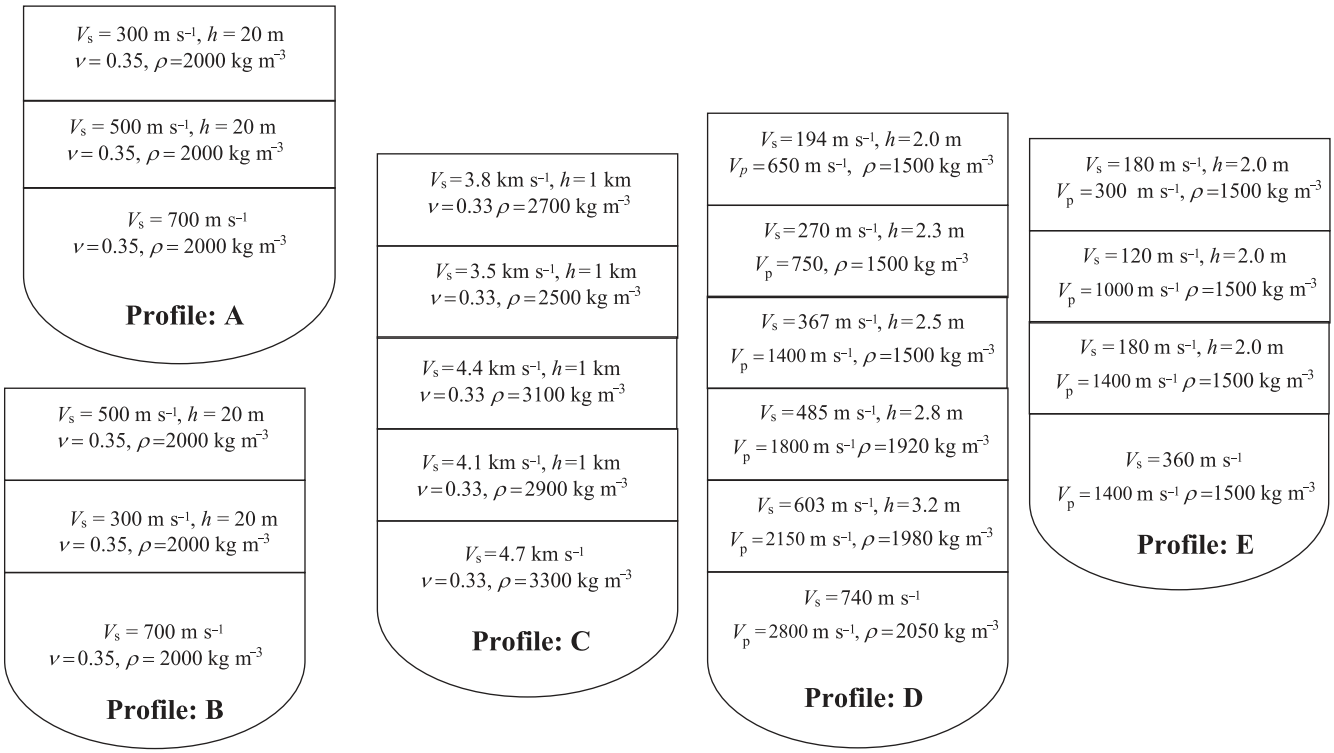

Figure 1. Five different profiles for analysis.

$$\boldsymbol{K}_{21} = \frac{(1-s^2)}{2D}\begin{bmatrix} \frac{1}{s}(rsS^r - S^s) & (C^r - C^s) \\ -(C^r - C^s) & \frac{1}{r}(rsS^s - S^r) \end{bmatrix} \quad (3d)$$

In the above terms, $C^r = \cosh(\kappa rh)$, $S^r = \sinh(\kappa rh)$, $C^s = \cosh(\kappa sh)$, and $S^s = \sinh(\kappa sh)$.

For the elastic half space,

$$\mathbf{K}_H = 2kG\left\{\frac{(1-s^2)}{2(1-rs)}\begin{bmatrix} r & 1 \\ 1 & s \end{bmatrix} - \begin{bmatrix} 0 & 1 \\ 1 & 0 \end{bmatrix}\right\}. \quad (4)$$

The horizontal wavenumber (κ) is expressed in terms of the phase velocity (V), that is,

$$\kappa = \frac{\omega}{V}, \ \omega = \kappa V, \quad (5)$$

$$\text{in which case, } r = \sqrt{1 - \left(\frac{V}{V_p}\right)^2}, \ s = \sqrt{1 - \left(\frac{V}{V_s}\right)^2}, \quad (6)$$

where V_p and V_s refer to the dilatational and shear wave velocities of the half space. A significant simplification of the DSM was achieved using the thin layer method (TLM) (Kausel and Roësset 1981). In the TLM, the physical layers of the medium are discretized into thin layers such that the thickness of any thin layer is kept much smaller as compared to the characteristic wavelength of the propagating wave. The primary advantage of the TLM is that the impedance matrix transforms from transcendental to algebraic. The impedance matrix turns out to be solely a function of the horizontal phase velocity and the wavenumber. If the subsurface comprises of n horizontal layers excluding the lowermost elastic half space, the applied external loads and global displacement vectors are finally correlated using the global stiffness matrix

$$\mathbf{F}_{(2n+2)\text{x}1} = \mathbf{K}_{(2n+2)\text{x}(2n+2)}\mathbf{U}_{(2n+2)\text{x}1}. \quad (7)$$

The global stiffness matrix can be established by doing the assembly operation of the local layer stiffness matrices.

It has been shown by Kausel and Roësset (1981) that the stiffness matrix **K** for a given layer can be presented in the following form:

$$\mathbf{K} = \mathbf{A}\kappa^2 + \mathbf{B}\kappa + \mathbf{C} - \omega^2\mathbf{M}. \quad (8)$$

Here, **A**, **B**, **C**, and **M** are the block-tridiagonal, symmetric matrices that become solely a function of material properties of the layers and their thicknesses; these stiffness matrices are given by Kausel and Roësset (1981).

To obtain the full wave spectra for different modes of wave propagation, the problem needs to be framed as a free vibration problem, that is, $\boldsymbol{P} = \mathbf{0}$, which implies $\boldsymbol{KU} = \mathbf{0}$ or $\boldsymbol{K} = \mathbf{0}$ since $\boldsymbol{U} \neq 0$. It is solved as an eigenvalue problem for evaluating the parameter ω in term of k or vice versa. Either way, the solution of the quadratic eigenvalue problem $|\mathbf{K}| = 0$ can be readily established. The MATLAB library routine *polyeig* was used for solving this quadratic eigenvalue problem. The solution generally yields real and complex eigenvalues. All layers were assumed to have no damping since the magnitude of damping hardly affects the results (Kumar 2011). Numerically negative real and complex eigenvalues are simply rejected (Kumar and Naskar 2017). One important consideration is to allocate the appropriate values for the parameter V, namely, the common phase velocity of the modes. The value of $V < V_s < V_p$ will be feasible otherwise the parameters r and s in equation (6) will

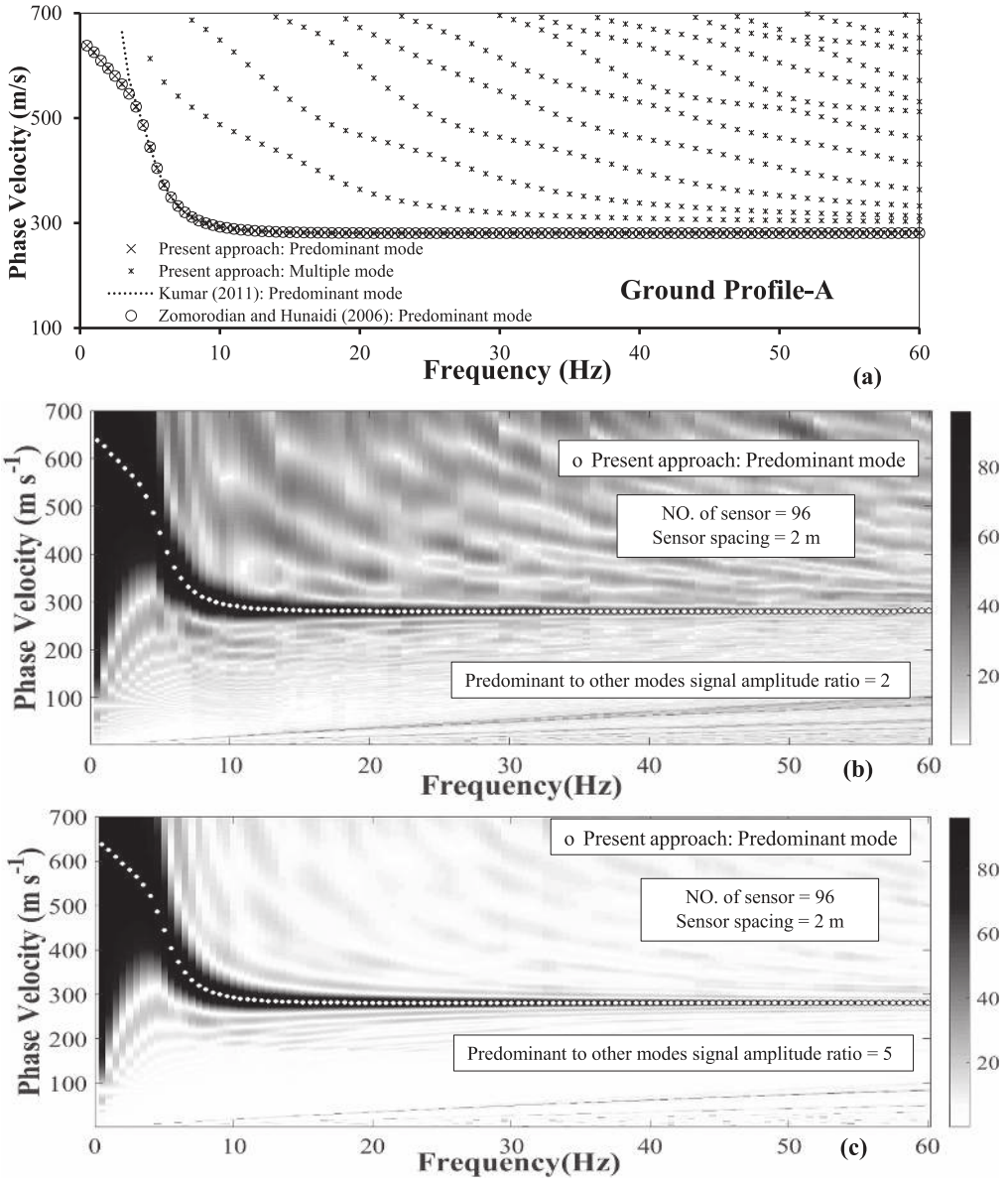

Figure 2. For profile A. (a) A comparison of the present approach with those given by Zomorodian and Hunaidi (2006), and Kumar (2011). (b) Predominant mode from the present approach and multiple modes from the MASW using an amplitude ratio of 2. (c) Predominant mode from the present approach and multiple modes from the MASW using an amplitude ratio of 5.

yield complex eigenvalues, and the analysis would no longer provide real eigenvalues. At the opposite extreme, the phase velocity cannot be arbitrarily small, but is likely to equal or exceed the smallest Rayleigh wave velocity in any layer. This then provides a bandwidth over which V must be varied while searching the complete wave dispersion spectrum. After the eigenvalue problem is solved numerically, one will find a set of frequencies $f = \omega/2\pi = f(V)$ that are compatible with the phase velocity.

To establish the predominant mode, an eigenvector must be examined for each admissible eigenvalue. The eigenvector provides a set of the interlayer displacement vector **U**. Each eigenvector is normalized with respect to the absolute maximum value from a set of all interlayer displacements. For each eigenvalue (mode), there will be a corresponding normalized eigenvector. The eigenvalue that predicts the maximum value of the normalized vertical displacement at the free surface is said to yield the predominant mode. This criterion is used as the basis to determine the predominant mode from a set of all admissible modes, which were obtained earlier as a solution of the corresponding quadratic eigenvalue problem.

3. Results and comparisons

In order to demonstrate the effectiveness of proposed technique, five different ground profiles, as shown in figure 1, were chosen. These profiles were named from A to E. The following details have been provided for different layers of

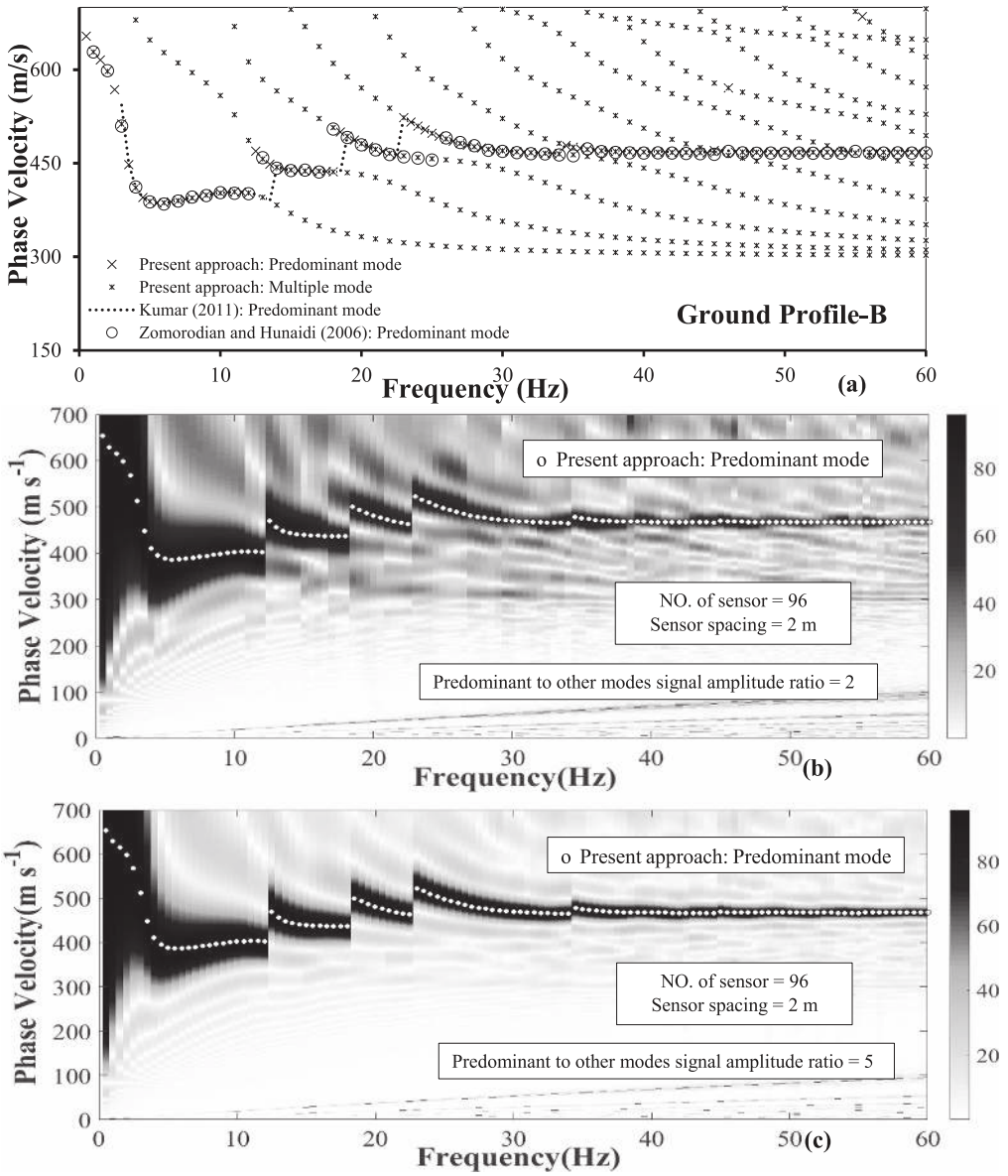

Figure 3. For profile B. (a) A comparison of the present approach with those given by Zomorodian and Hunaidi (2006), and Kumar (2011). (b) Predominant mode from the present approach and multiple modes from the MASW using an amplitude ratio of 2. (c) Predominant mode from the present approach and multiple modes from the MASW using an amplitude ratio of 5.

these profiles: (i) thickness (h), (ii) mass density (ρ), (iii) shear wave velocity (V_s), and (iv) primary wave velocity (V_p)/Poisson ratio (ν). For the purpose of performing the analysis, the values of the damping ratio were specified to be zero in all cases. Profiles A and B were taken from the paper of Zomorodian and Hunaidi (2006). Both of these profiles comprise of two layers, each having a thickness of 20 m. These two layers are underlaid by an elastic half space. The value of V_s varies between 300 m s^{-1} and 700 m s^{-1}. Profile A is regular dispersive, whereas profile B is irregular dispersive since it comprises of a soft layer sandwiched between two stiff layers. Profile C has been chosen from the work of Strobbia (2003). This profile exhibits four layers lying above the half space. This profile is also irregular dispersive: the second and fourth layers have smaller values of V_s than the overlying stiff layer. Furthermore, each layer has a thickness of 1 km. The value of V_s ranges between 3.5 km s^{-1} and 4.7 km s^{-1}. Profile D has been chosen from the paper by Xia *et al* (1999). It is regular dispersive with V_s increasing continuously with depth. It has five layers overlying the elastic half space. Layer thickness varies between 2.0 m and 3.2 m. The value of V_s changes between 194 m s^{-1} and 740 m s^{-1}. Profile E has been taken from the work of Tokimatsu *et al* (1992). It has three layers overlying the elastic half space. This soil profile is also irregular dispersive: the second layer has a smaller value of V_s than the overlying stiff layer. The value of V_s varies between 120 m s^{-1} and 360 m s^{-1}.

For all five different profiles, first the multiple modal dispersion curves were generated, and then the dispersion curves associated with predominant modes were established

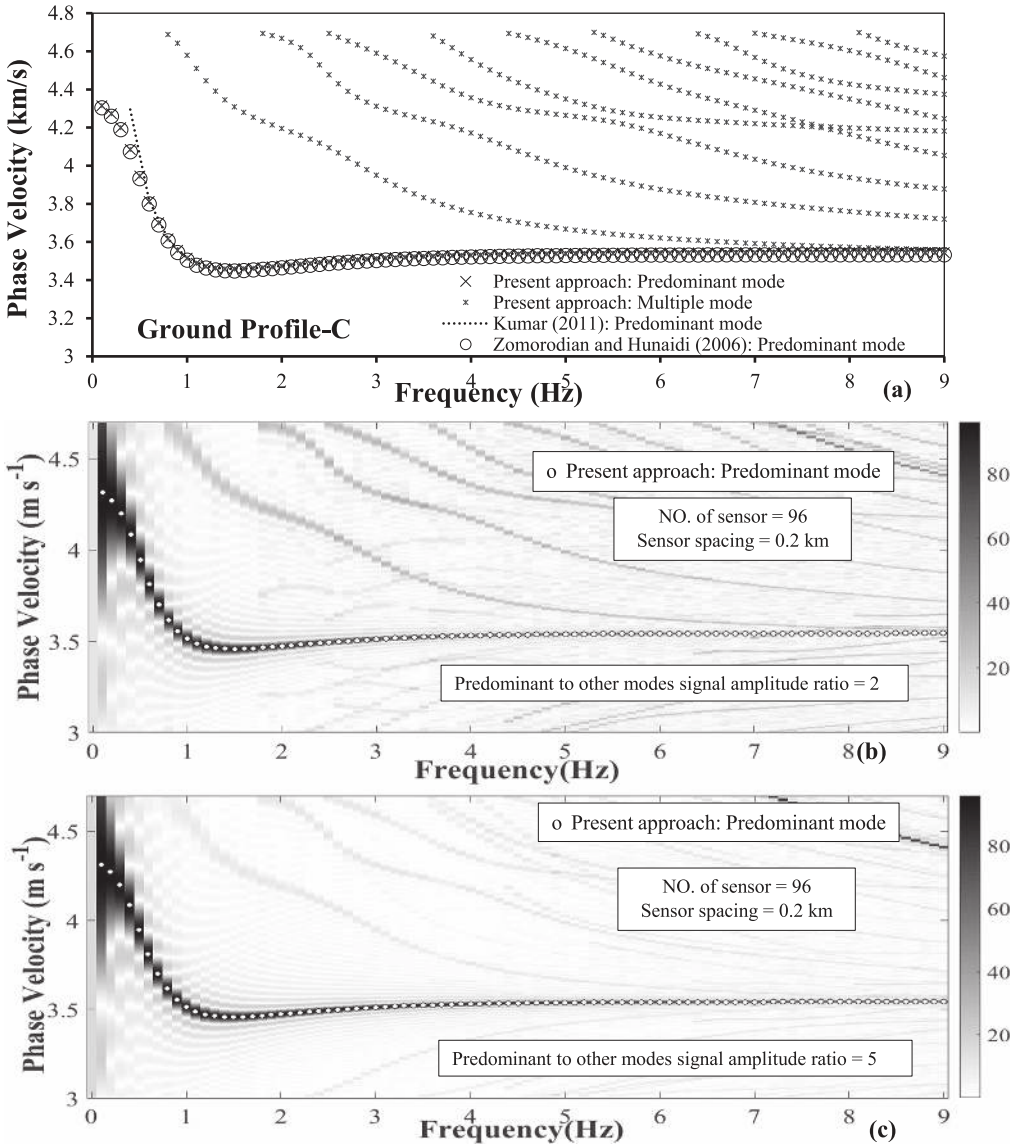

Figure 4. For profile C. (a) A comparison of the present approach with those given by Zomorodian and Hunaidi (2006), and Kumar (2011). (b) Predominant mode from the present approach and multiple modes from the MASW using an amplitude ratio of 2. (c) Predominant mode from the present approach and multiple modes from the MASW using an amplitude ratio of 5.

based on the proposed approach. The obtained results in all the cases were also compared with those using (i) the maximum flexibility approach of Zomorodian and Hunaidi (2006), and (ii) the finite difference approach of Kumar (2011). In addition, a comparison was also made with dispersion plots (i) computed by the superposed mode as predicted by Tokimatsu *et al* (1992) for profile E, and (ii) measured in the site by Xia *et al* (1999) for profile D. The results for all five profiles are presented in 1 part (a) of figures 2–6.

Note that the predominant mode predicted by the present approach compares closely with those presented by Zomorodian and Hunaidi (2006), and Kumar (2011). At very low frequencies, the phase velocity predicted by Kumar (2011) was found to be a little greater compared to the present analysis. This is on account of a very large number of layers needed for the discretization in the analysis by Kumar (2011) associated with greater wavelengths. For an irregular dispersive profile, the analysis by Zomorodian and Hunaidi (2006) gave slightly different results in a region where mode shifts occur. However, in general, the present analysis and the approach of Zomorodian and Hunaidi (2006) were found to compare quite well with each other. For the ground profile D, the measured dispersion curve as reported by Xia *et al* (1999) was found to compare well with the present analysis. A little difference was again noted between the two analyses in a region where the mode shifts occurs between the first two modes. For profile E, the superposed mode predicted by Tokimatsu *et al* (1992) was found to compare well with the present analysis. For a frequency smaller than about 5 Hz, the

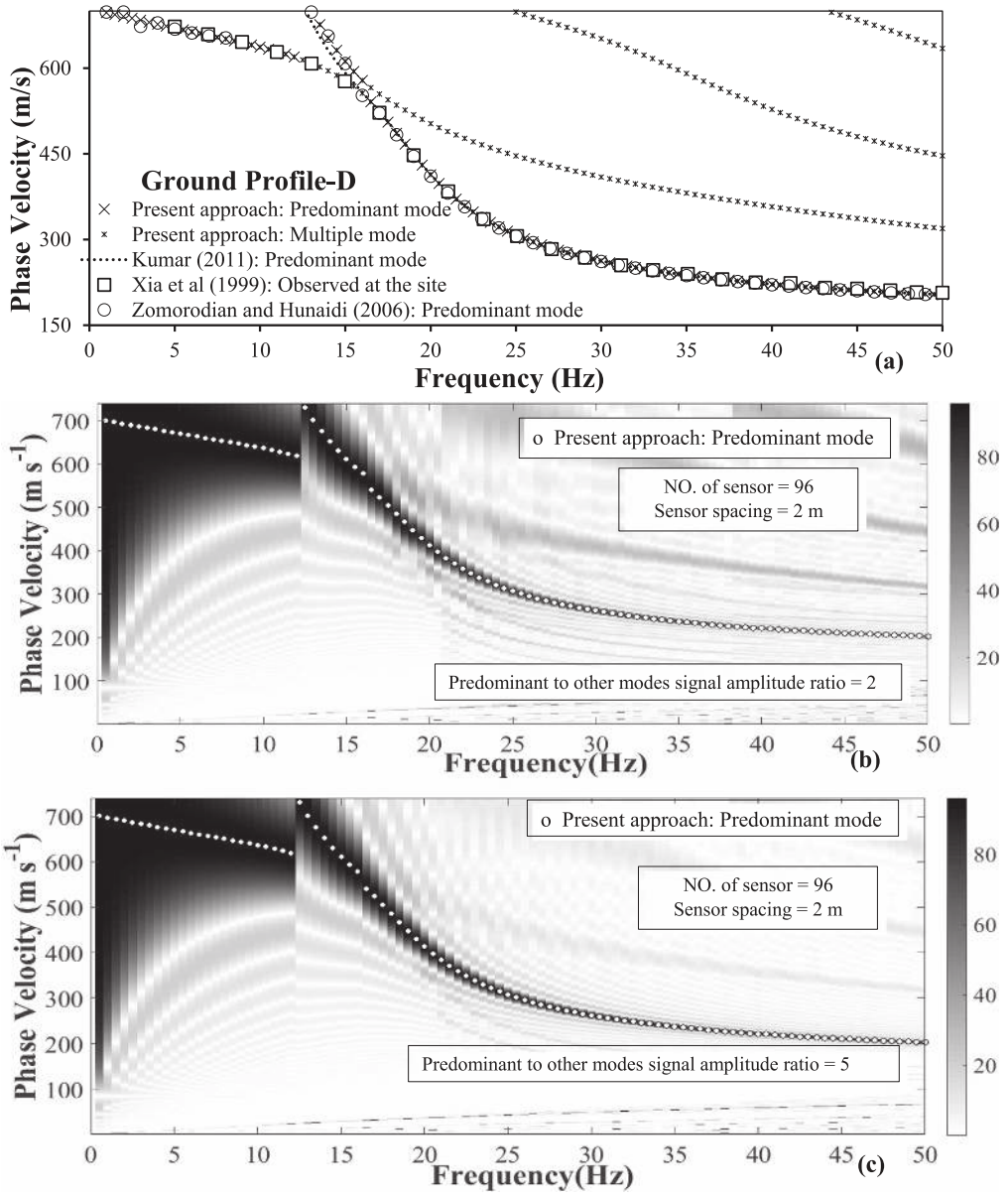

Figure 5. For profile D. (a) A comparison of the present approach with those given by Xia *et al* (1999), Zomorodian and Hunaidi (2006), and Kumar (2011). (b) Predominant mode from the present approach and multiple modes from the MASW using an amplitude ratio of 2. (c) Predominant mode from the present approach and multiple modes from the MASW using an amplitude ratio of 5.

superposed mode predicted by Tokimatsu *et al* (1992) lies along the second modal curve, whereas the present analysis provides the predominant mode along the first modal plot.

By using the method proposed by Park and Miller (2008), for given dispersion plots associated with multiple modes as shown in part (a) of figures 2–6, synthetic signals associated with 96 channels were generated. Corresponding to a given combination of receiver spacing and source location, the method of generation of the synthetic seismogram is summarized in the appendix. These synthetic data were then used to establish the multimodal dispersion plots on the basis of the MASW technique (Xia *et al* 1999).

Multiple dispersion plots established on the basis of the MASW technique for five different chosen soil profiles are shown in parts (b) and (c) of figures 2–6. Parts (b) and (c) are associated by keeping the ratio of the amplitude of the predominant mode to all other modes equal to 2 and 5, respectively.

It can also be seen from parts (b) and (c) of figures 2–6 that when the amplitude ratios of the predominant mode to the other modes are changed from 2 to 5, the visibility of the other modal dispersion plots, as compared to the predominant mode, become quite poor. In other words, this observation implies that if the energy of the modes other than the predominant ones is not really very strong, it is going to be quite unlikely that multiple modes will be observed at the site by using a lesser number of sensors even if the soil is not regular dispersive.

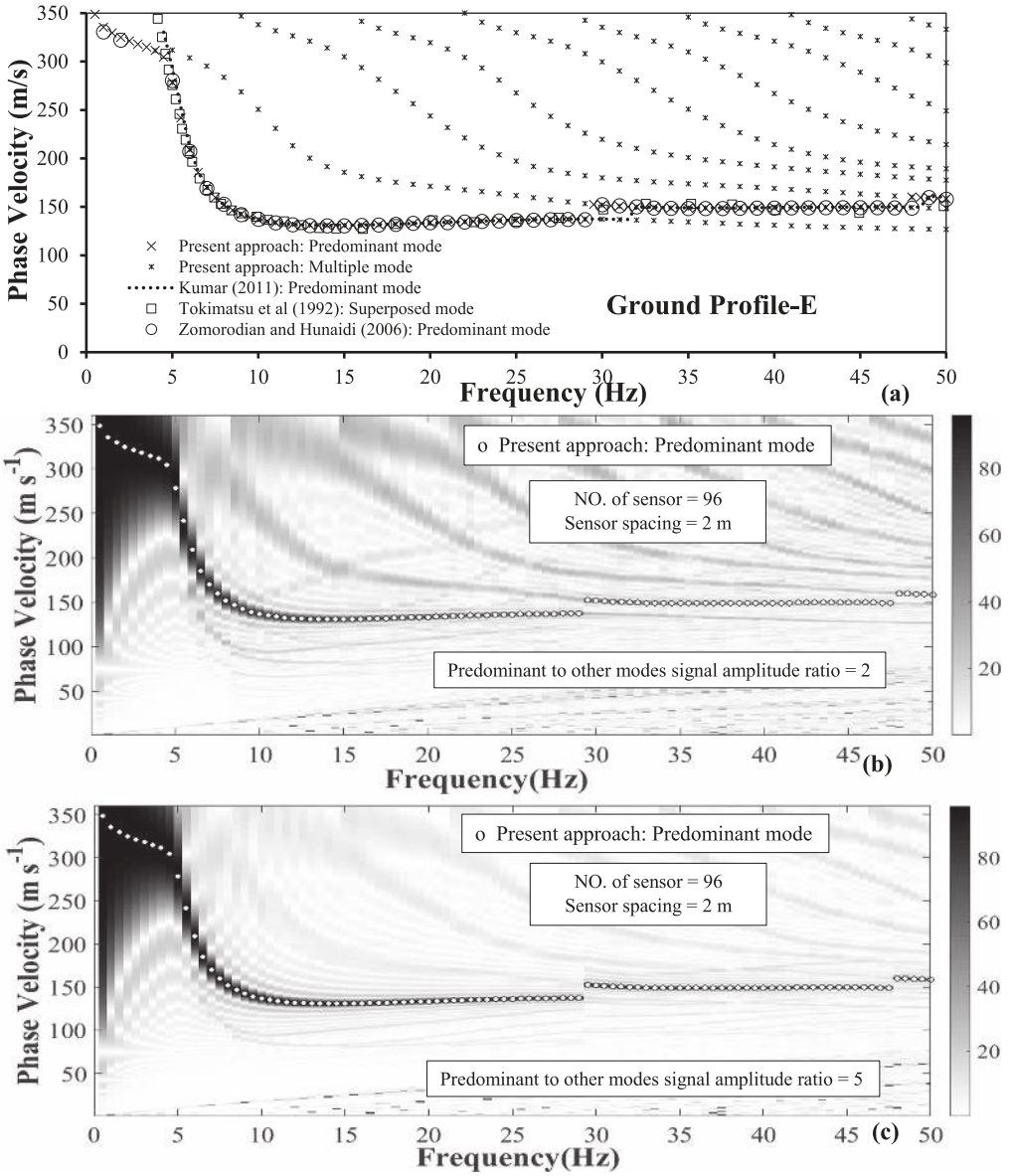

Figure 6. For profile E. (a) A comparison of the present approach with those given by Tokimatsu *et al* (1992), Zomorodian and Hunaidi (2006), and Kumar (2011). (b) Predominant mode from the present approach and multiple modes from the MASW using an amplitude ratio of 2. (c) Predominant mode from the present approach and multiple modes from the MASW using an amplitude ratio of 5.

4. Energy associated with different modes

The energy carried by any propagating wave for a given frequency becomes directly proportional to the square of the corresponding displacement amplitude (Richart *et al* 1970). In the multimodal dispersion plots, the ratio of the energies (E_i/E_p) associated with a given modal dispersion plot to that with the predominant mode can be determined by simply taking the squares of the corresponding displacement amplitudes' ratios. For illustration, multimodal dispersion plots associated with profile B were chosen. Five different frequencies, namely, 10 Hz, 20 Hz, 30 Hz, 40 Hz, and 50 Hz, were selected. The values of E_i/E_p were marked for the dispersion plots associated with different modes at these five selected frequencies. Corresponding results are illustrated in figure 7; this is a reproduction of figure 3(a) with the energies' ratios marked. It can be seen that the value of E_i/E_p remains in unity for all predominant modes cases, and this ratio decreases continuously with an increase in the absolute difference between the numbers associated with a given mode and the predominant mode.

5. Remarks

The approach presented in this paper can be directly used in an inversion procedure. One needs to compare the dispersion plot obtained from a given site with that numerically generated on the basis of the proposed forward analysis for the selected input parameters of the different layers. The values of

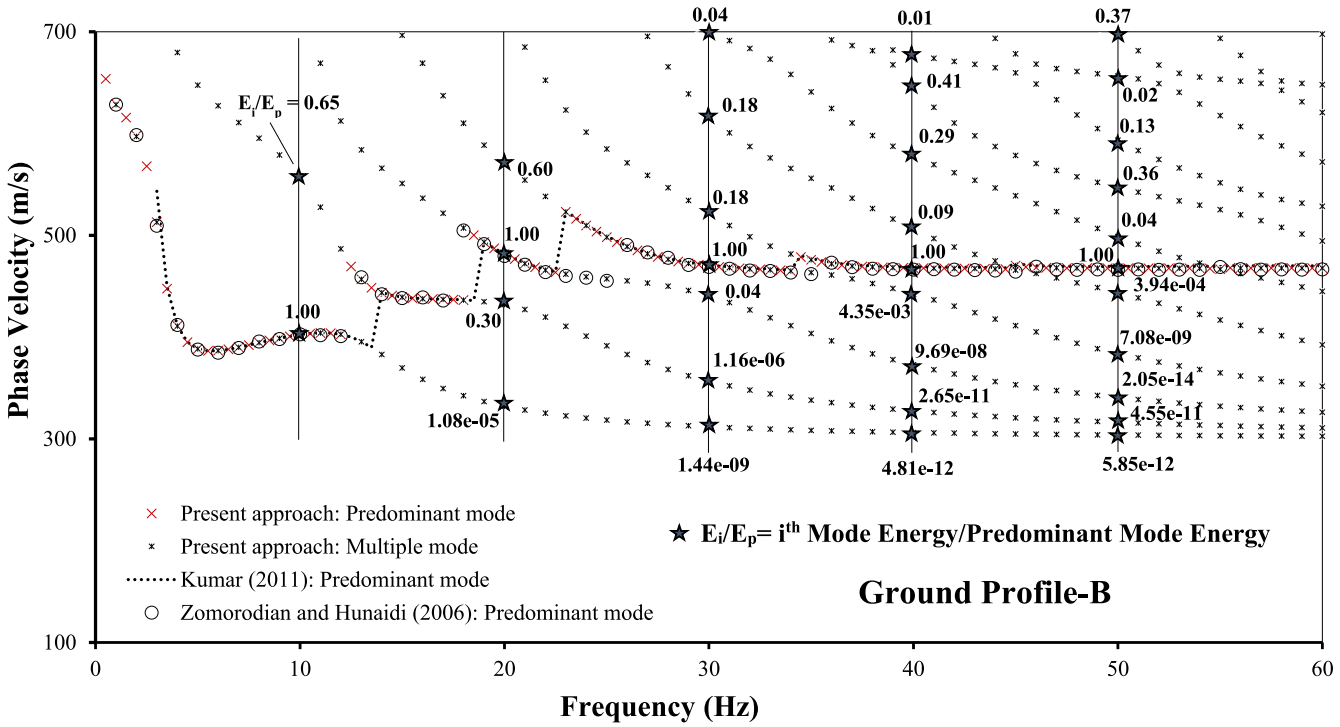

Figure 7. For profile B, a comparison of the energies at the predominant mode to other modes for a set of selected frequencies.

the input parameters must be updated until the difference between the two dispersion plots becomes almost negligible. This will eventually predict the required input parameters of the ground profile.

6. Conclusions

Based on the DSM approach, predominant modal dispersion plots are determined while dealing with the problem of Rayleigh wave propagation. The accuracy of the proposed technique has been checked by comparing the results from the literature. The present method compares favorably with existing approaches. The present analysis is based on the popular DSM approach, and the solution can be easily obtained by examining the eigenvectors (displacements). It is also noted that when the energy of the predominant mode is much greater compared to the other modes, it is quite unlikely that all the different multiple modes other than the predominant one will be observed in a site with the usage of a lesser number of receivers; in such cases, the determination of a predominant modal dispersion plot will be quite useful in predicting the shear wave velocity profile of the media.

Acknowledgments

The authors gratefully acknowledge the financial support provided by (i) the Department of Science and Technology, India (Grant No # SR/S3/MERC/072/2010) and (ii) the Department of Atomic Energy, BRNS (Grant No # 2012/36/22-BRNS/1589), India.

Appendix

Synthetic seismogram generation

A surface wave of circular frequency ω, mode number m, amplitude a_k^m, phase delay δ_k, and associated with an arbitrary source location $L_k = \{x_k, y_k\}$, is represented in a frequency domain as follows:

$$S_k^m(\omega) = a_k^m \mathrm{e}^{-\mathrm{j}(\omega+\delta_k)}. \quad \text{(A1)}$$

The signature $R_i^{m,k}(\omega)$ of this source signal on the ith receiver located at $L_i = \{x_i, y_i\}$ is written as follows:

$$R_i^{m,k}(\omega) = A_{ik}^m P_{ik}^m S_k^m(\omega), \quad \text{(A2)}$$

where $A_{ik}^m = \frac{\mathrm{e}^{(\alpha l_{ik})}}{l_{ik}}$ and $P_{ik}^m = \mathrm{e}^{\frac{\mathrm{j}\omega l_{ik}}{C_\omega^m}}$; the terms A_{ik}^m and P_{ik}^m imply amplitude and phase modulation factors. In the above expressions, α is an attenuation factor, and is equal to $\frac{\omega}{C_\omega^m Q}$, Q is the quality factor, C_ω^m is the phase velocity for the mth mode for the frequency ω, and $l_{ik} = \sqrt{(x_i - x_k)^2 + (y_i - y_k)^2}$. In the case of a multimodal surface wave, the resultant wave at the ith receiver is calculated by summing over all modes (M):

$$R_i^k(\omega) = \sum_{m=1}^{M} R_i^{m,k}(\omega). \quad \text{(A3)}$$

Accordingly, the synthetic seismogram for the ith receiver in a time domain due to the kth source can be written simply by taking an inverse Fourier transform of $R_i(\omega)$:

$$r_i(t) = FFT^{-1}[R_i(\omega)]. \quad \text{(A4)}$$

Note that while generating the synthetic seismogram, the effects of geometric damping and the attenuation factor are taken into account.

References

Dunkin J W 1965 Computation of modal solutions in layered, elastic media at high frequencies *Bull. Seismol. Soc. Am.* **55** 335–58

Gabriels P, Snider R and Nolet G 1987 *In situ* measurements of shear-wave velocity in sediments with higher-mode Rayleigh waves *Geophys. Prospecting* **35** 187–96

Ganji V, Gucunski N and Nazarian S 1998 Automated inversion procedure for spectral analysis of surface waves *J. Geotech. Geoenvir. Eng. ASCE* **124** 757–70

Gucunski N and Woods R D 1992 Numerical simulation of the SASW test *Soil Dyn. Earthq. Eng.* **11** 213–27

Haskell N A 1953 The dispersion of surface waves on multilayered media *Bull. Seismol. Soc. Am.* **43** 17–34

Hossain M M and Drnevich V P 1989 Numerical and optimization techniques applied to surface waves for back calculation of layer moduli *Nondestructive Testing of Pavements and Backcalculation of Moduli* (ASTM Special Technical Publication 1026) ed A J Bush and G Y Baladi (West Conshohocken, PA: ASTM) (https://doi.org/10.1520/STP19836S)

Jones R 1962 Surface wave technique for measuring the elastic properties and thickness of roads: theoretical development *Br. J. App. Phys.* **13** 21–9

Kausel E and Roësset J M 1981 Stiffness matrices for layered soils *Bull. Seismol. Soc. Am.* **71** 1743–61

Kumar J 2011 A study on determining the theoretical dispersion curve for Rayleigh wave propagation *Soil Dyn. Earthq. Eng. Elsevier* **31** 1196–202

Kumar J and Naskar T 2015 Effects of site stiffness and source to receiver distance on surface wave tests' results *Soil Dyn. Earthq. Eng. Elsevier* **77** 71–82

Kumar J and Naskar T 2017 A fast and accurate method to compute dispersion spectra for layered media using a modified Kausel-Roësset stiffness matrix approach *Soil Dyn. Earthq. Eng. Elsevier* **92** 176–82

Kumar J and Naskar T 2017 Resolving phase wrapping by using sliding transform for generation of dispersion curves *Geophysics* **82** 127–V136

McMechan G and Yedlin M J 1981 Analysis of dispersive waves by wave field transformation *Geophysics* **46** 869–74

Nazarian S 1984 *In-situ* determination of elastic moduli of soil deposits and pavement systems by spectral-analysis-of-surface-waves method *PhD Thesis* University of Texas, Austin

Nazarian S and Desai M R 1993 Automated surface wave method: field testing *J. Geotech. Eng. ASCE* **119** 1094–111

Nolet G and Panza G F 1976 Array analysis of seismic waves: limits and possibilities *Pure Appl. Geophys.* **114** 776–90

Park C B, Miller R D and Xia J 1998 Imaging dispersion curves of surface waves on multichannel record *SEG Technical Program Expanded Abstracts 1998* pp 1377–80

Park C B, Miller R D and Xia J 1999 Multichannel analysis of surface waves *Geophysics* **64** 800–8

Park C B and Miller R D 2008 Roadside passive multichannel analysis of surface waves (MASW) *J. Environ. Eng. Geophys.* **13** 1–11

Richart F E, Hall J R and Woods E D 1970 *Vibrations of Soils and Foundations* (Englewood Cliffs, NJ: Prentice Hall)

Strobbia C 2003 Surface wave methods: acquisition, processing and inversion *Dottorato di Ricerca in Geoingegneria Ambientale* Politecnico Di Torino

Thomson W T 1950 Transmission of elastic waves through a stratified solid medium *J. Appl. Phys.* **21** 89–93

Tokimatsu K, Tamura S and Kojima H 1992 Effect of multiple modes on Rayleigh wave dispersion characteristics *J. Geotech. Eng. ASCE* **118** 1529–43

Xia J, Miller R D and Park C B 1999 Estimation of near-surface shear-wave velocity by inversion of Rayleigh waves *Geophysics* **64** 691–700

Zomorodian S M A and Hunaidi O 2006 Inversion of SASW dispersion curves based on maximum flexibility coefficients in the wave number domain *Soil Dyn. Earthq. Eng.* **26** 735–52